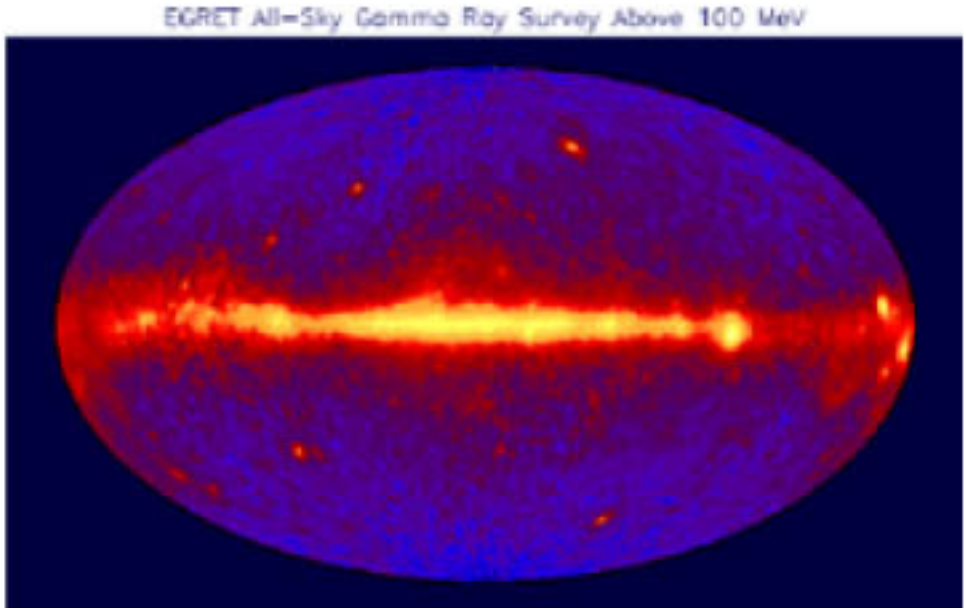


Figure 1.8: The as sky seen by the EGRET satellite above 100 MeV. Most of the emission comes from the region of the galactic plane but at higher galactic latitudes are some objects which are extragalactic. Many of them are Blazars.

***minutes for Mkn 421***. This can be partially explained by a high Doppler factor (Equ. 1.6) of the relativistically moving source and by small emission regions (which are tens of AU (1 AU$\simeq$ 15 light minutes)) .

But even with small emission regions and high Doppler factors ***common SSC models have problems*** to explain this fast variability of Mkn 421. New theories try to explain this behavior. They range from small ***conical sub shock fronts*** inside the jet (Model for Mkn 421 [Sal98]), ***laminar rather than spherical emission regions*** [Mas99], and ***modulation*** of the soft photon field for Compton up-scattering via a hot spot in the accretion disc [Bed96].

It should be possible to differentiate between these models by examining the ***correlation*** of x-ray flux and light curve measurements of x-ray satellites and the GeV-TeV emission. If the soft photons for up-scattering come from the accretion disc, there should only be a very weak correlation of the flares in the UV/x-ray and the TeV range. This would point to a modulation version.

If there is a ***strong correlation***, like in the case of Mkn 501, this points toward the ***SSC model***, possibly with ***conical shocks*** or ***thin laminal shocks*** traversing the jet (See Fig. 1.6).

A very precise measurement of a ***flare of Mkn 421*** in the x-ray region (see Fig. 1.9) has been recorded by ***ASCA in April 1998*** which seems to show a correlation between x-ray flux and $\gamma$-ray flux. The x-ray and TeV curves of Fig. 1.9 match perfectly, when superposed. In the analysis chapter the correlation between the x-ray flux as measured by ASCA in 1998 and various TeV instruments will be examined in detail. The ASCA x-ray flux measurement seems to show two components. A slow flare component ($\sim$7 day duration) and a fast (sub-day) flare component.

## 1.3 The Gamma Ray Horizon

The universe is filled with isotropically distributed diffuse photons of low energy from the microwave energy range (i.e. cosmic microwave background or CMB) peaking at 2.7 K up

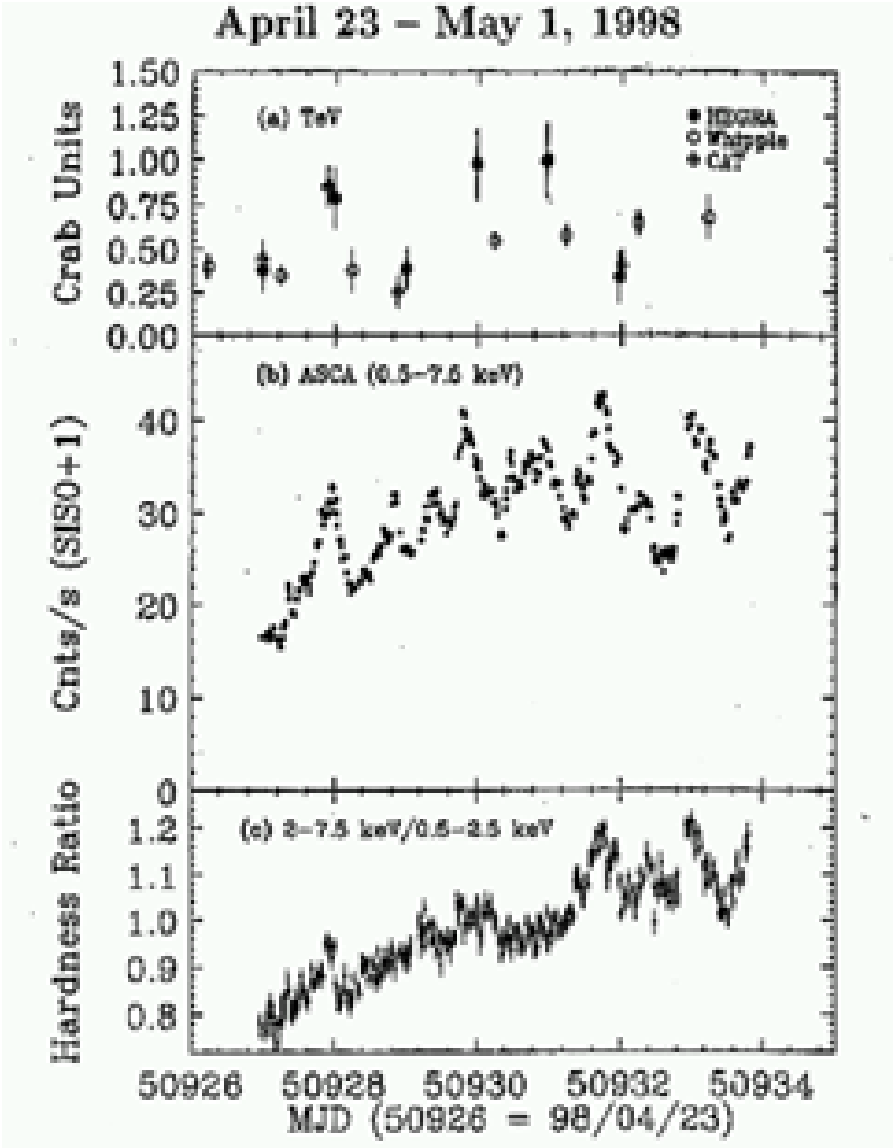


Figure 1.9: Multi-wave length observation of Mkn 421 in 1998 with ASCA in the x-ray region and with several Cherenkov telescopes in the TeV energy range. The integrated TeV flux is measured in units of the (constant) crab flux and the x-ray flux (rate) in counts/sec. When the x-ray curve is superposed on the TeV curve it can be seen that the TeV curve follows the x-ray curve. This will be discussed in detail in chapter B.

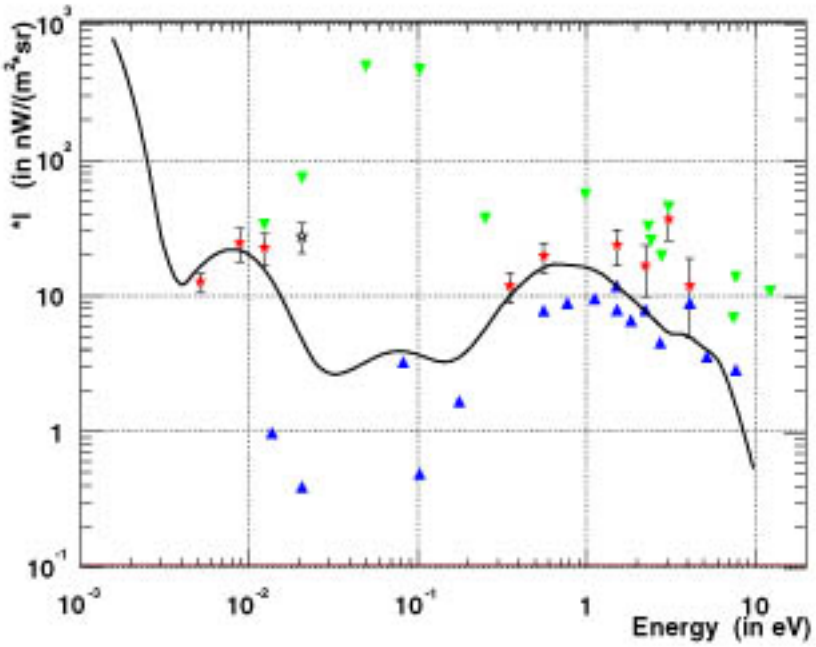


Figure 1.10: Actual measurements of the cosmic infrared background. The green points are upper limits, the blue ones are lower limits from galaxy counts, the red ones are trusted measurements and the hollow black one is a tentative measurement. The data has been taken from [Hau01]. The model is from T. Kneiske and K. Mannheim [Kne02]. The increase of the energy density on the left side is the CMB.

to the infrared (i.e. ***cosmic infrared background*** or CIB) and the visible light range. The interaction of the very high energy (VHE) $\gamma$'s with the low energy background radiation (VLE photons) plays an important role in gamma ray astronomy.

This interaction ***limits*** the observable energy range as a function of $\gamma$-energy. Therefore one would expect ***cutoffs*** in the spectra. This attenuation effect of the VHE $\gamma$ on their way to the earth, which depends on the red shift of the source, is called ***gamma ray horizon*** (a more precise definition will be given later, Equ. 1.23). The source of the interaction is electron positron pair production from high energy and low energy photons.

$$\gamma_{VHE} + \gamma_{VLE} \rightarrow e^+ + e^- \tag{1.14}$$

The VLE photons have different origin. The 2.7 K microwave background radiation is a remnant of the Big Bang with a thermal spectrum from $10^5$ $\mu$m to $10^3$ $\mu$m. Another important contribution from the ***far infrared (***100 $\mu$***m) to the UV (0.1*** $\mu$***m)*** comes from redshifted star light that has been occurring throughout the history of the universe. Star formation processes in the early universe play an important role here. Thus the precise measurement of the spectrum of these background photons provides detailed information about the history of our universe.

Unfortunately the direct measurements of the extragalactic infrared background by satellite borne instruments are ***very difficult*** because of foreground infrared light in our galaxy, i.e. dust reflecting the (infrared) light from the sun and stars inside the galaxy. The actual measurements of the infrared background can be seen in Fig. 1.10. The numbers have been taken from [Hau01]. The region between a few $\mu$m and 100 $\mu$m has not been measured at all. Only upper and lower limits exist. The lower limits come from galaxy counts and are hard limits [Hau01]. The plotted curve shows a models developed by T.

Kneiske and K. Mannheim [Kne02]. This model is quite complex and involve convolutions of measured star formation rates, initial mass functions and the history of dust and light densities.

In order to calculate the absorption that VHE photons experience we need to ***fold*** the cross section of the pair-production process with the low energy photon density. ***The cross section*** for the process described in Equ. 1.14 is (in $cm^2$) [Ste95]:

$$\sigma\left(E\left(z\right),\varepsilon\left(z\right),x\right) = 1.25\cdot 10^{-25}\left(1-\beta\right)\times \tag{1.15}$$

$$\left[2\beta\left(\beta^2-2\right)+\left(3-\beta^4\right)\cdot ln\left(\frac{1+\beta}{1-\beta}\right)\right] \tag{1.16}$$

where

$$\beta=\sqrt{1-\frac{2\left(m\,c^2\right)}{E\varepsilon x(1+z)^2}} \tag{1.17}$$

$E$ is the energy of the gamma ray photon, $\varepsilon$ is the energy of the soft photon, $z$ is the redshift of the source and $x=(1-\cos(\vartheta))$ is the angle between the photon directions. ***The threshold energy condition*** is

$$E\varepsilon x\left(1+z\right)^2>2\left(mc^2\right)^2 \tag{1.18}$$

The cross section, plotted in the range between 100 $\mu$m and 0.1 $\mu$m, for a 1 TeV, a 3 TeV, a 10 TeV and a 30 TeV photon from a head on collision (solid line) and averaged over all angles (dashed line), together with the measurements of the infrared background can be seen in Fig. 1.11. This time the photon density instead of the energy density has been plotted, because this is the quantity which determines the absorption. This plot illustrates which soft photon range interacts with which high energy photon. The higher energy photons (10 TeV and 30 TeV) fall into an energy range of the cosmic ray background which has not been measured yet. The measured spectrum of Mkn 421 puts strong constraints and upper limits on the soft photon density in that range.

To get the optical depth $\tau$ (attenuation to $e^{-\tau}$ of the original flux) for one specific energy, one must ***fold*** the cross section with the cosmic infrared spectrum and average over the whole solid angle $\Omega$ of photon collision angles and integrate this result over the redshift $z$. Since the object of this work (Mkn 421 with $z$=0.03, z$\ll$ 1) is relatively close to the earth (440 million light years away), it is not necessary to integrate over $z$, which simplifies the relation.

The absorption probability per unit length (in cm) is [Ste01, Bla01]:

$$\frac{d\tau}{dl}=\frac{1}{2}\int_{-\frac{\pi}{2}}^{\frac{\pi}{2}}\sin\vartheta d\vartheta\int_{\frac{2m^2c^4}{E(1-\cos\vartheta)}}^{\infty}d\varepsilon\frac{dn}{d\varepsilon}\sigma\left(E,\varepsilon,(1-\cos\vartheta)\right) \tag{1.19}$$

$\frac{dn}{d\varepsilon}$ is the ***differential soft photon density*** (in units of number of photons per $cm^3$and eV) and must be calculated from the cosmic infrared background spectrum (Intensity $\nu\frac{dI}{d\nu}=\nu I_\nu$ (in units of nW/$(m^2sr)$)) in the following way:

$$\varepsilon^2\frac{dn}{d\varepsilon}=\frac{4\pi}{ec}\quad\nu I_\nu \tag{1.20}$$

whereas $\varepsilon$ denotes the photon energy in eV. The distance to the object is, to first order, (for z$\ll$ 1):

$$l=\frac{c\cdot z}{H_0} \tag{1.21}$$

$H_0=68\pm6\frac{km}{sec\cdot Mpc}$ is the Hubble constant (1 pc = $3.086\cdot10^{18}$ cm). Finally the attenuation of the flux becomes:

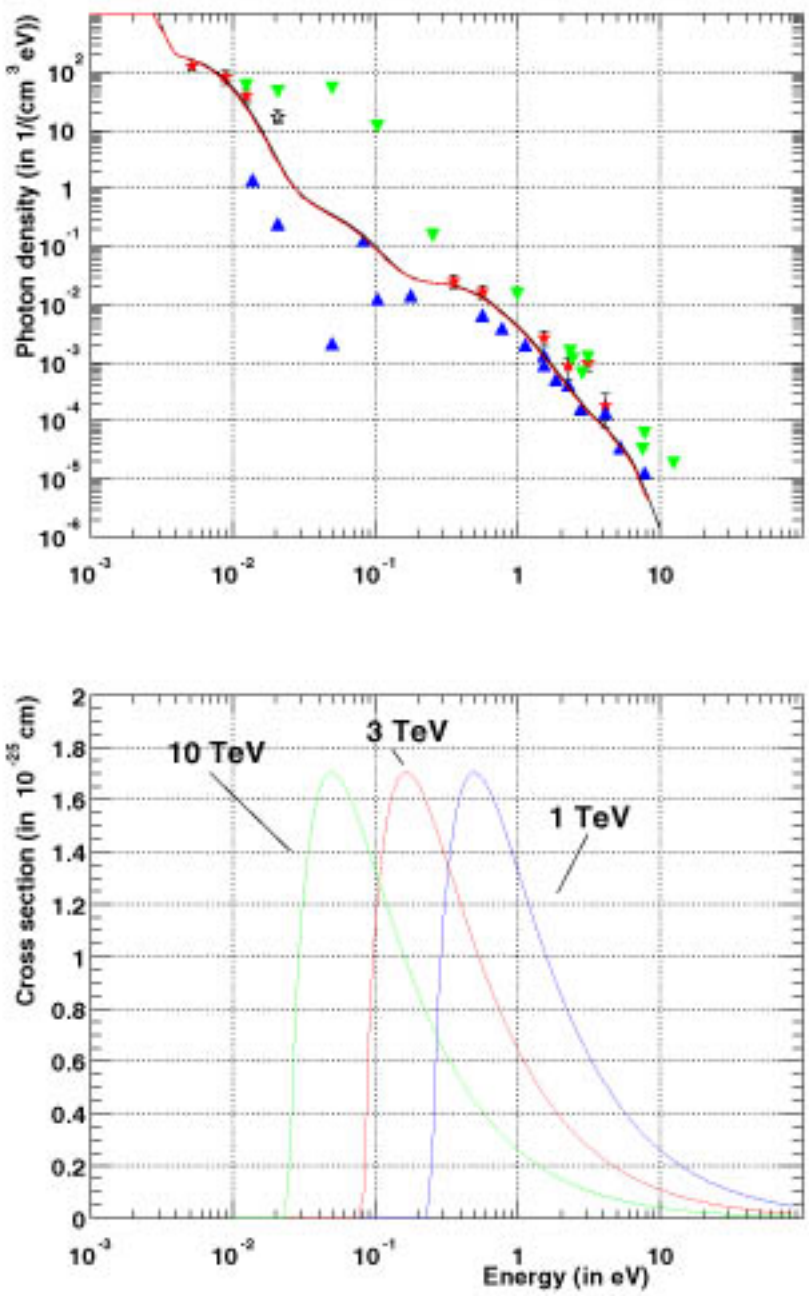


Figure 1.11: a) The upper plot displays, for comparison, ***the cosmic infrared background measurements*** in terms of differential photon density together with different models of [Kne01] of the CIB. The blue points are lower limits, the green ones are upper limits and the red points are accepted measurements. b) The lower plot shows the ***cross section*** for a 1 TeV (blue), a 3 TeV (red), a 10 TeV (green) and a 30 TeV photon from a head-on collision (solid line) and averaged over all collision angles (dashed line).

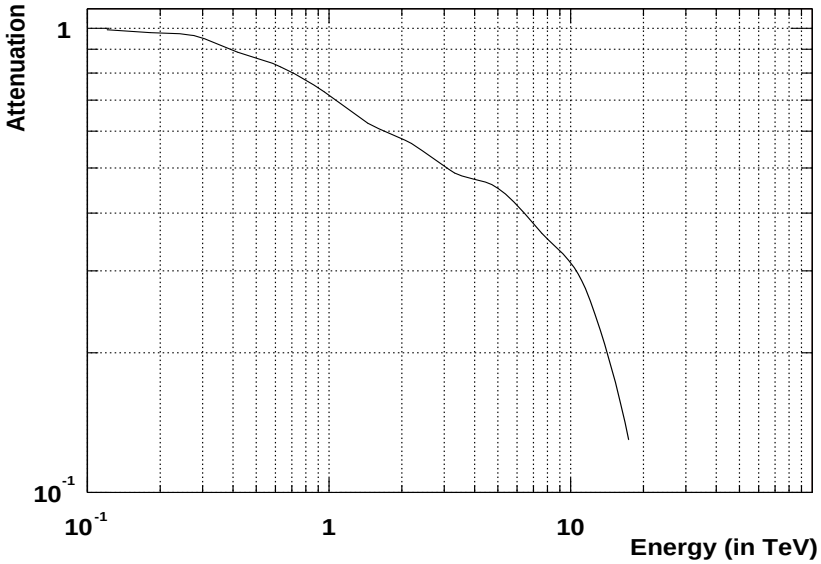


Figure 1.12: The ***attenuation*** of TeV gammas originating from Mkn 421 and according to the models [Kne02] shown in Fig. 1.11. According to these models the attenuation starts above 1 TeV but the effect becomes ***significantly*** strong after 10 TeV.

$$A = e^{-\frac{d\tau}{dl} * l} \tag{1.22}$$

Fig. 1.12 shows the ***attenuation*** of gammas originating from Mkn 421 at $z$=0.031 for the models shown in the Fig. 1.11. It should be noted that the ***cutoff*** that has been observed, for example, in the spectrum of Mkn 501 ($z$=0.034) [Ste01] can have two possible reasons. One is the ***absorption*** due to the cosmic infrared background. The other is that the cutoff could be an ***intrinsic feature*** of the BL LAC emission spectrum. As of today, it is not clear which of these hypotheses is actually responsible for the cutoff. It could even be a ***mixture of both***. These possibilities will be discussed later in the last Chapter concerning the analysis of the Mkn 421 flares of 2001.

The gamma ray horizon (Fig. 1.13) is defined as the red shift for which

$$\tau\,(E, z) = 1 \tag{1.23}$$

This is the distance $z$ for which the attenuation becomes $1/e$.

## 1.4 Theory of air showers

There are two ways of detecting gamma photons. One is such that the gamma photons are detected directly in space. This is done via the x-ray and gamma-ray satellites. Satellites have a limited detection area of a few $m^2$ and have therefore a limited sensitivity. The second possibility uses the ***atmosphere*** as a part of the ***detector***.

The VHE gamma flux is so low, that huge detection areas ($\sim 10^5\ m^2$) are needed to collect a reasonable number of events per observation time. Above 10 GeV the collection area of current satellite borne $\gamma$-detectors is too small and only the method of ***ground based instruments*** can be used. This section is therefore dedicated to explain how the atmosphere reacts with cosmic rays.

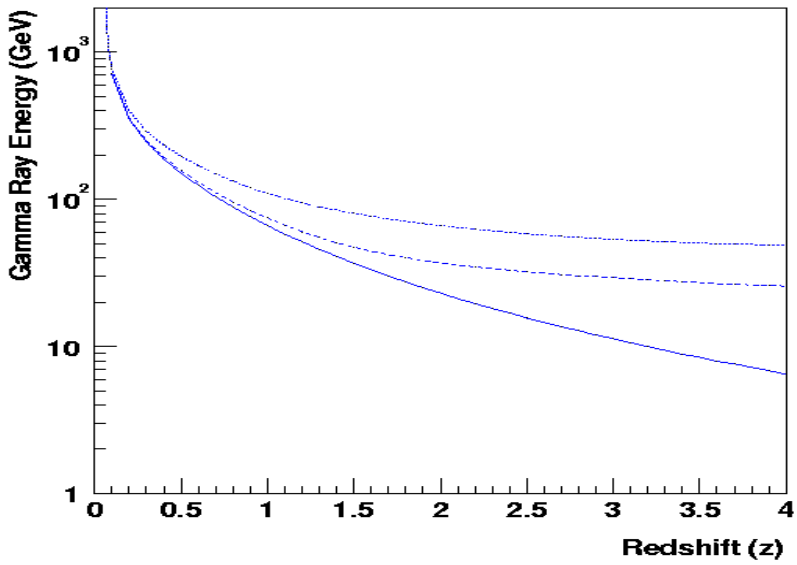


Figure 1.13: The gamma ray horizon plotted against the red shift. Taken from [Bla01]. As of today, it is not exactly known where the horizon is located. The different curves show the attenuation for different cosmic parameters and CIB models. The location of the gamma ray horizon gives important information about CIB and is a very actual field of research.

When cosmic rays enter the atmosphere, they generate so-called air showers. The cosmic ray particles interact with the molecules of the atmosphere by hadronic and electromagnetic interaction. ***Electrons, muons and $\gamma$'s interact electromagnetically***, which means they generate secondary particles by pair production and bremsstrahlung. The secondary particles are mostly again non-hadronic particles as ***Electrons, muons and $\gamma$'s***.

Hadronic CR, namely ***Protons and ionized nuclei*** interact via the ***hadronic interaction***, which means that they produce as secondary particles mainly $\pi$'s, $\mu$ and K's. These latter particles either decay or produce more secondary particles by hadronic interaction. $\pi^0$ decay almost instantly into two photons and therefore ***feed the electromagnetic component*** of an hadronic shower.

In this way, a cascade of secondary particles is initiated. These highly relativistic particles, mainly electrons, emit Cherenkov radiation during their travel through the atmosphere. The air showers extend, depending on their energy, from the upper levels of the atmosphere down to sea level (see Fig. 1.14).

There are two types of air showers: The ***electromagnetic type***, which have ***no*** hadronic particles and the ***hadronic showers***, which contain all types of particles.

### 1.4.1 Electromagnetic cascades

The electromagnetic shower is easier to discuss mathematically because to first order it ***only*** contains ***electromagnetic particles***, consisting of ***electrons***, ***muons*** and ***photons***. Photons are produced by ***bremsstrahlung*** and by the ***annihilation*** of positrons. Electrons and positrons are produced by ***pair production***. The energy of the original photon is transfered to the secondary particles whose number ***increases*** continuously.

The particles ***lose energy*** by ***multiple scattering*** and also by ***ionization*** of the surrounding air molecules. The number of particles increases until the shower maximum. From that point on the average particle energy decreases because of energy losses due to ionization and bremsstrahlung. The cascade equations can be found in [Gai90]. For the

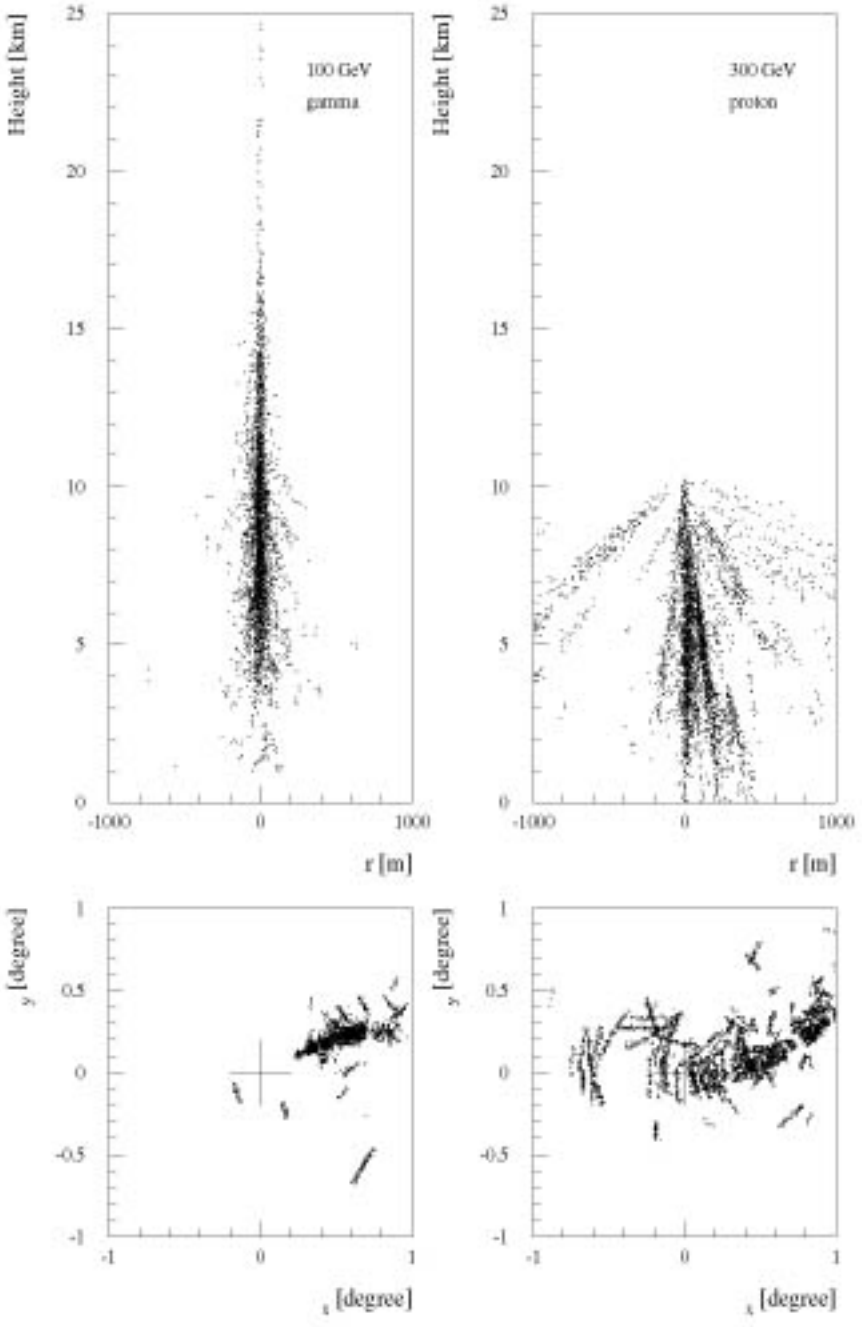


Figure 1.14: a) Top row: Images of two typical air showers, for a gamma photon (left side) and a proton (right side) , calculated by Monte Carlo simulation and 2) Bottom row: their Cherenkov image seen by a telescope, taken from [Kra01]